Journal of Materials Science & Technology 122 (2022) 10–19

Contents lists available at ScienceDirect

Journal of Materials Science & Technology

journal homepage: www.elsevier.com/locate/jmst

Research Article

Surface photodynamic ion sterilization of ITO-Cu_2O/ZnO preventing touch infection

Zexin Liu[a], Xiangmei Liu[b,*], Zhenduo Cui[a], Yufeng Zheng[c], Zhaoyang Li[a,**], Yanqin Liang[a], Xubo Yuan[a,**], Shengli Zhu[a], Shuilin Wu[a,c,**]

[a] School of Materials Science & Engineering, the Key Laboratory of Advanced Ceramics and Machining Technology by the Ministry of Education of China, Tianjin University, Tianjin 300072, China
[b] School of Life Science and Health Engineering, Hebei University of Technology, Tianjin 300401, China
[c] School of Materials Science & Engineering, Peking University, Beijing 100871, China

ARTICLE INFO

Article history:
Received 3 December 2021
Revised 21 December 2021
Accepted 27 December 2021
Available online 20 March 2022

Keywords:
Antibacterial
Cu_2O
ZnO
Contact infection
Photodynamic ion sterilization

ABSTRACT

Pathogenic microbial infections are threatening the people's health and even life. The most common channel of infections can be caused by skin contact, especially hand touching facilities such as touching screen. In this work, Cu_2O covered with ZnO nanofilm was prepared on the surface of indium tin oxide conductive glass by electrodeposition and the followed atomic layer deposition process. This composite coating had a light transmittance of 71.5%, which met the light transmission needs of touch screen device. Electron spin resonance spectra showed that composite materials can generate more reactive oxygen species (ROS) than a single component under solar light irradiation. This was because a *p-n* junction with a built-in electric field was formed at the interface after Cu_2O contacting with ZnO. In the process of photocatalysis, photogenerated electrons and holes migrated at the interface driven by the built-in electric field, which promoted the separation of carriers. The antibacterial rate against *Staphylococcus aureus* reached 92.5% after 3 min of light irradiation with simulated sunlight due to the synergy of ROS and Cu ions, Zn ions. Therefore, this work may provide a potential method for antibacterial application of preventing hand touch infections.

1. Introduction

In recent years, the problem of bacterial infections in commonly used facilities such as elevator handrails and subways, etc. has attracted more and more attention because pathogenic microbial infections have been threatening public health and people's life [1,2]. These infected facilities will become a breeding ground for various microorganisms when they are used frequently and not thoroughly cleaned [3]. In fact, most of the bacteria on the surface of public equipment originate from human hand contact [4,5]. Studies had shown that the hand surface possessed > 150 unique species-level bacterial system types [6]. These bacteria also include spreading pathogens that can cause a wide spectrum of diseases such as gastrointestinal and respiratory diseases [7].

Currently, the commonly used surface sterilization methods are chemical disinfectants and ultraviolet (UV) disinfection [8]. Chemical disinfectants include hypochlorite, hydrogen peroxide, ethanol solution, and etc., which can kill bacteria quickly and effectively. However, these chemicals need to be sprayed regularly to maintain the sterilization effect. In addition, these chemicals can also cause environmental pollutions including air, water and soil pollutions. UV disinfection as a "no-touch" technologies can reduce surface contamination caused by bacteria [9]. However, the UV disinfection will cause adverse damage to human health. Therefore, it is necessary to build an anti-infective surface on the hand touching surface to prevent infection caused by hand contact.

In recent years, some emerging antibacterial methods such as photothermal sterilization [10–13], photodynamic sterilization [14–19], physical puncture [20], ultrasound excited bacteria-killing [21–24], and microwave assisted disinfection [25–27], have been devel-

* Corresponding author.
** Corresponding authors at: School of Materials Science & Engineering, the Key Laboratory of Advanced Ceramics and Machining Technology by the Ministry of Education of China, Tianjin University, Tianjin 300072, China.
E-mail addresses: Liuxiangmei1978@163.com (X. Liu), zyli@tju.edu.cn (Z. Li), xbyuan@tju.edu.cn (X. Yuan), shuilin.wu@gmail.com (S. Wu).

https://doi.org/10.1016/j.jmst.2021.12.064
1005-0302/

Table 1
Shortcoming of other antibacterial methods for preventing touch infection.

Antibacterial methods	Disadvantages of being used to preventing touch infection
Chemical disinfectants	1 Needing to be sprayed regularly 2 Causing environmental pollutions
UV disinfection	1 Cause adverse damage to human health
Photothermal sterilization	1 Overheating cause certain damage to some specific equipment 2 Not suitable for people to continue to use due to overheating
Physical puncture	1 Depending on the motility of bacteria and the nature of nanoneedle itself 2 The nanoneedle will break when the finger keeps touching
Ultrasound and microwave excited bacteria-killing	1 Requiring special equipment 2 High-cost

oped. Photothermal treatment requires high heat (generally greater than 50 °C) to kill bacteria [28]. But overheating can cause certain damage to some specific equipment. At the same time, the surface temperature is too high for people to continue to use these devices. Physical puncture can use nanoneedle to puncture bacteria [29]. But the effect of physical puncture largely depends on the motility of bacteria and the nature of nanoneedle itself [30]. Therefore, it is impractical to apply physical puncture sterilization on the surfaces frequently touched by hands. Microwave and ultrasonic excited sterilization require specific equipment, which obviously increases the cost of preventing surface contact infection Table 1. summarizes the shortcoming of these antibacterial methods for preventing touch infection. In contrast, photodynamic sterilization has unique advantages. The photocatalytic process can be described as follows. Light with the appropriate wavelength stimulates the photosensitizer to react with oxygen (O_2) and other substances to produce cytotoxic reactive oxygen species (ROS), which in turn leads to the death of bacteria [31]. Among them, light is a cheap energy source. At the same time, O_2 and other substances are also inexhaustible resources. Furthermore, ROS has broad-spectrum sterilization properties and does not develop bacterial resistance [32,33]. The release of metal ions allows the constructed antibacterial surface to kill bacteria in dark conditions. In this regard, a photodynamic ion sterilization method was selected to impart antibacterial properties to hand touching surfaces.

In the past decades, some researchers used the photocatalysis of cuprous oxide (Cu_2O) to kill bacteria on hand touching surfaces [34]. But pure Cu_2O had the limitation of rapid recombination of electrons and holes and low photocatalytic efficiency [35]. In order to solve these problems, a Cu_2O/Zinc oxide (ZnO) heterojunction was built on indium tin oxide (ITO) conductive glass by electrodeposition and atomic layer deposition (ALD) process. The results showed that the photocatalytic performance of the composite material was significantly improved due to the formation of *p-n* heterojunction [36]. After irradiating using solar light for 3 min, the antibacterial rate against *Staphylococcus aureus* (*S. aureus*) of the composite material reached 92.5%. The bactericidal effect was attributed to the synergy of ROS and Cu ions, Zn ions. At the same time, when phosphate buffered saline (PBS) aqueous solution was used to simulate the actual use environment of the antibacterial surface, it was found that the ZnO nanofilms deposited by ALD had a certain protective effect on Cu_2O and slowed down the corrosion of Cu_2O in aqueous solution. In addition, the light transmittance of the composite group can reach 71.5%, implying the potential antibacterial application of this composite material on touch screen surface.

2. Experimental

2.1. Materials

ITO conductive glass (20 mm × 30 mm, 1.1 mm in thickness) was purchased from South China Science & Technology Company. Copper (II) sulfate pentahydrate ($CuSO_4$) and potassium hydroxide (KOH) were purchased from Tianjin Kemiou Chemical Reagent Co., Ltd (China). Lactic acid (C_3H_6O) and Potassium phosphate dibasic (K_2HPO_4) were purchased from Tianjin C&S Biochemical Technology Co., Ltd (China). Ethanol, and acetone were purchased from Sinopharm Chemical Reagent Co. (China).

2.2. Pretreated of ITO conductive glass surface

ITO conductive glass was employed as the main substrate. The substrates were ultrasonically cleaned for 20 min in acetone, ethanol, and deionized water sequentially to remove contaminants.

2.3. Preparation of the Cu_2O particles

The Cu_2O particles were electrodeposited on the surface of ITO conductive glass from a basic solution of lactate stabilized copper sulfate electrolyte [37]. Specifically, 1.50 g of $CuSO_4$, 4.08 g of K_2HPO_4 and 12.68 g of lactic acid were dissolved in 100 ml of H_2O.

The pH of the electrolyte was adjusted to 12 by KOH (2 M) solution. Cu_2O particles were deposited at a constsant current density of -0.1 mA/cm^2 (Galvanostatic mode) for 20 min using an electrochemical workststion (GRMEY Reference 600, China) with a three-electrode configuration (a Pt mesh served as the counter electrode and an Ag/AgCl electrode as the reference electrode). During deposition, the electrolyte was maintained at 30 °C. The samples obtained after electrodeposition were called ITO-Cu_2O.

2.4. Prepared of the ZnO nanofilms

The ZnO nanofilms were deposited on the ITO conductive glass and ITO-Cu_2O substrates by ALD (MNT-P-100-43, China) using diethyl zinc ((C_2H_5)$_2$Zn, DEZ) and H_2O as zinc and oxygen precursors, respectively. The substrate temperature was maintained at 180 °C during deposition. Each cycle consisted of precursor exposure and N_2 purging following a sequence of DEZ: N_2: H_2O: N_2 with a corresponding duration of 0.02: 10: 0.02: 25 s. The reaction was repeated for 200 cycles to obtain the ZnO nanofilms. The samples with ZnO nanofilms deposited on ITO conductive glass and ITO-Cu_2O substrate are called ITO-ZnO and ITO-Cu_2O/ZnO.

2.5. Characterization

The light transmittance of the sample was tested with a blue light transmittance tester (Shenzhen Speedre Technology CO., Ltd). The surface topography of samples was analyzed by Scanning Electron Microscope (SEM) (JSM-7800F, Japan). Transmission Electron Microscope (TEM) (JEOL-2100F, Japan) equipped with corresponding elemental mapping and selected area electron diffraction (SAED) was employed to observe the microstructure and crystal structure of the samples. X-ray photoelectron spectroscopy (XPS) (ThermoFisher Scientific 250Xi, USA) was conducted for elemental analysis. All the binding energies were calibrated by the C 1s peaks located at 284.8 eV. Ultraviolet-visible-NIR (UV-vis-NIR) absorption spectra and diffuse reflectance absorption spectra were employed using a UV-2700 spectrophotometer (Shimadzu).

2.6. Photoelectrochemical measurement

The electrochemical testing of the samples was undertaken using an electrochemical workstation (CHI660E, China) with a three-electrode system, where a saturated calomel electrode, a Pt electrode and each sample served as the reference, counter and working electrode, respectively. All measurements were processed in 0.5 M Sodium sulfate (Na_2SO_4) solution at 25 °C. The photocurrents were recorded in the presence and absence of xenon lamp (PLS-SXE300/300UV) irradiation. Under xenon lamp (PLS-SXE300/300UV) irradiation, the electrochemical impedance spectroscopy (EIS) was measured from 10 kHz to 1 Hz, with an amplitude of 5 mV.

2.7. Detection of ROS

Electron spin resonance (ESR) spectra were performed by a JES-FA200 spectrometer. 5,5-Dimethyl-1-pyrroline-N-oxide (DMPO) (Sigma) was used to trap hydroxyl radicals (•OH) and superoxide radical (•O_2^-). The ITO, ITO-Cu_2O, ITO-ZnO and ITO-Cu_2O/ZnO samples were immersed in 100 mM DMPO at ambient temperature under xenon lamp irradiation (PLS-SXE300/300UV).

2.8. Evaluation of the antibacterial activity

Pure ITO conductive glass was set as the control group and ITO-Cu_2O, ITO-ZnO, ITO-Cu_2O/ZnO constituted the experimental groups. 20 μL of the *S. aureus* suspension (3.5 × 10^4 CFU/ml) was added to each sample (20 mm × 20 mm). Afterwards, the samples were or were not irradiated with xenon lamp (PLS-SXE300/300UV) as the light source to explore sterilization. Illumination intensity is one sunlight intensity (100 mW/cm^2). Bacteria adhered to the samples was inverted on standard LB agar for 2 h and then the samples were taken down. The standard LB agar was incubated at 37 °C for another 20 h. The bacterial colonies were counted and the antibacterial ratio was calculated by the following formula: antibacterial ratio (%) = $(A - B)/A$, where A is the average number of bacterial colonies in the control group (ITO conductive glass sample, CFU/cm^2) and B is the average number of bacterial colonies in the experimental sample (CFU/cm^2). Three parallel samples from each group were used in the antibacterial test. In order to observe the morphology of the bacteria after the antibacterial experiment, the bacteria on the sample were fixed with a 2.5% glutaraldehyde solution for 40 min and dehydrated using graded ethanol solutions (20%, 40%, 60%, 80%, and 100%) for 15 min. After drying, the morphologies and microstructures were observed by SEM.

2.9. Water corrosion test

ITO-Cu_2O and ITO-Cu_2O/ZnO samples were socked in 0.01 M PBS for 0 h, 12 h, 24 h. The morphology of each sample was observed by SEM (JSM-7800F, Japan).

3. Results and discussion

As shown in Fig. 1(A), the Cu_2O/ZnO heterojunction can be prepared by deposition of Cu_2O particles on ITO conductive glass using electrodeposition followed by deposition of ZnO nanofilm on ITO-Cu_2O using atomic layer deposition (ALD). The size of the particles formed by electrodeposition and the thickness of ZnO nanofilms formed by ALD can be controlled by tuning the parameters. After Cu_2O and ZnO were deposited sequentially, the surface color of the material changed significantly, indicating that Cu_2O particles and ZnO nanofilm were successfully deposited on the substrate (Fig. 1(B)). When the ITO-Cu_2O/ZnO sample was placed on phone screen surface, the information of the phone can still be clearly seen (Fig. 1(C)). It implied that the system had potential antibacterial applications on the surface of touch screen device. Moreover, we did a light transmittance test on the prepared samples. As shown in Fig. 1(D), the light transmittance of ITO, ITO-Cu_2O and ITO- ZnO were maintained above 80%. The light transmittance of ITO-Cu_2O/ZnO was 71.5%, which can meet the daily light transmittance requirements of touch screen device. This also showed that the material had stronger light absorption properties than other groups, which was conducive to photocatalytic sterilization.

The surface morphologies of the synthesized materials were examined by SEM. The surface of ITO conductive glass was regular, with some small bumps evenly distributed (Fig. S1(A)). After depositing the ZnO nanofilm on ITO conductive glass, the surface of the material became smoother (Fig. S1(B)). It could be observed from Fig. 2(A) that the Cu_2O particles were uniform in size and evenly distributed on the ITO conductive glass surface. It can be seen from the enlarged view of Fig. 2(B), the Cu_2O particles were embedded on the ITO conductive glass, indicating that the Cu_2O particles were grown *in situ* on the ITO conductive glass. The Cu_2O particles had a regular square shape with a uniform side length of about 2 μm. The exposed crystal plane of Cu_2O was (100) crystal plane [34,38]. The surface of Cu_2O particles was smooth. After depositing the ZnO nanofilm, the size of the particles hardly changed (Fig. 2(C)). However, the particle surface became relatively rough. The rough surface film was the ZnO nanofilm. Elemental mappings of ITO-Cu_2O (Fig. S2) and ITO-Cu_2O/ZnO (Fig. S3) further proved the successful deposition of Cu_2O particles and ZnO

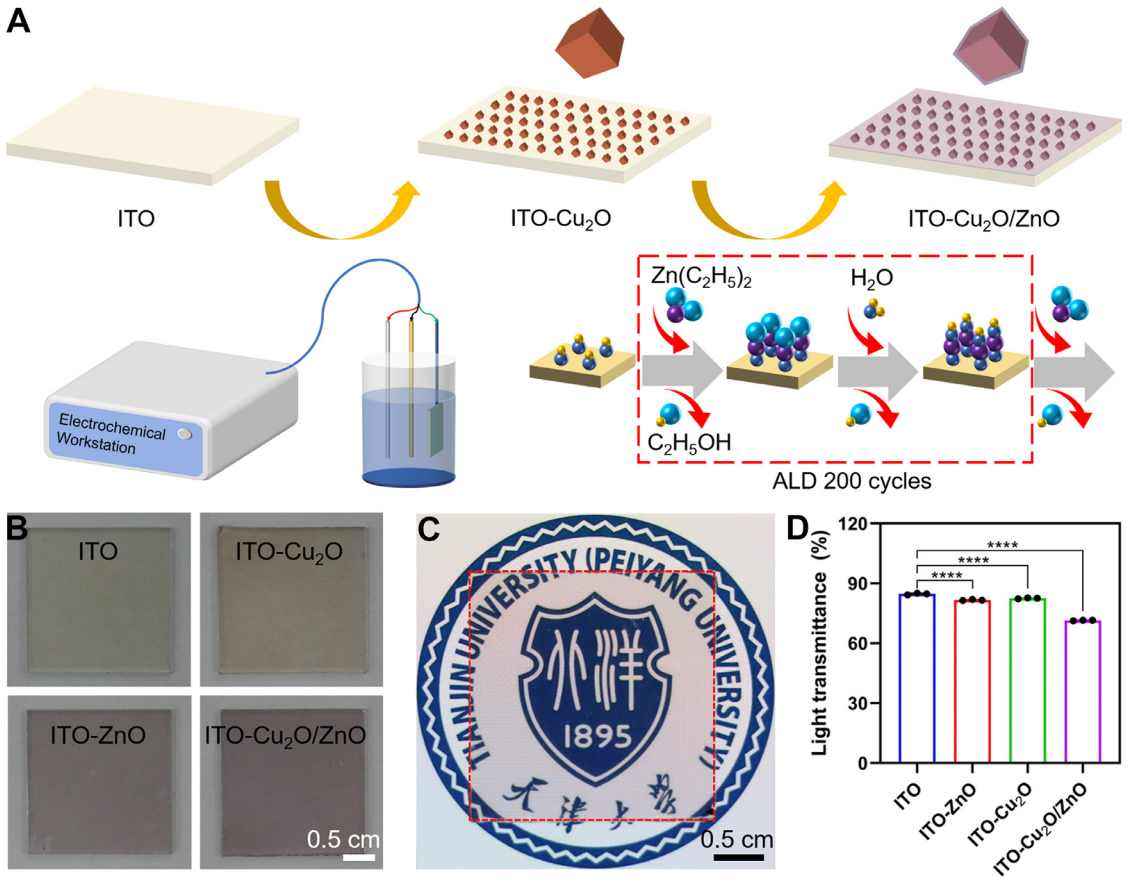

Fig. 1. (A) Schematic illustration of the fabrication process of the Cu_2O/ZnO heterojunction; (B) Photographs of each group of samples (Scale bar, 0.5 cm); (C) Photograph of the ITO-Cu_2O/ZnO sample placed on the surface of the phone (Scale bar, 0.5 cm); (D) Light transmittance of each group of samples. The error bar means ± standard deviations ($n = 3$ independent samples): $^{****}p < 0.0001$.

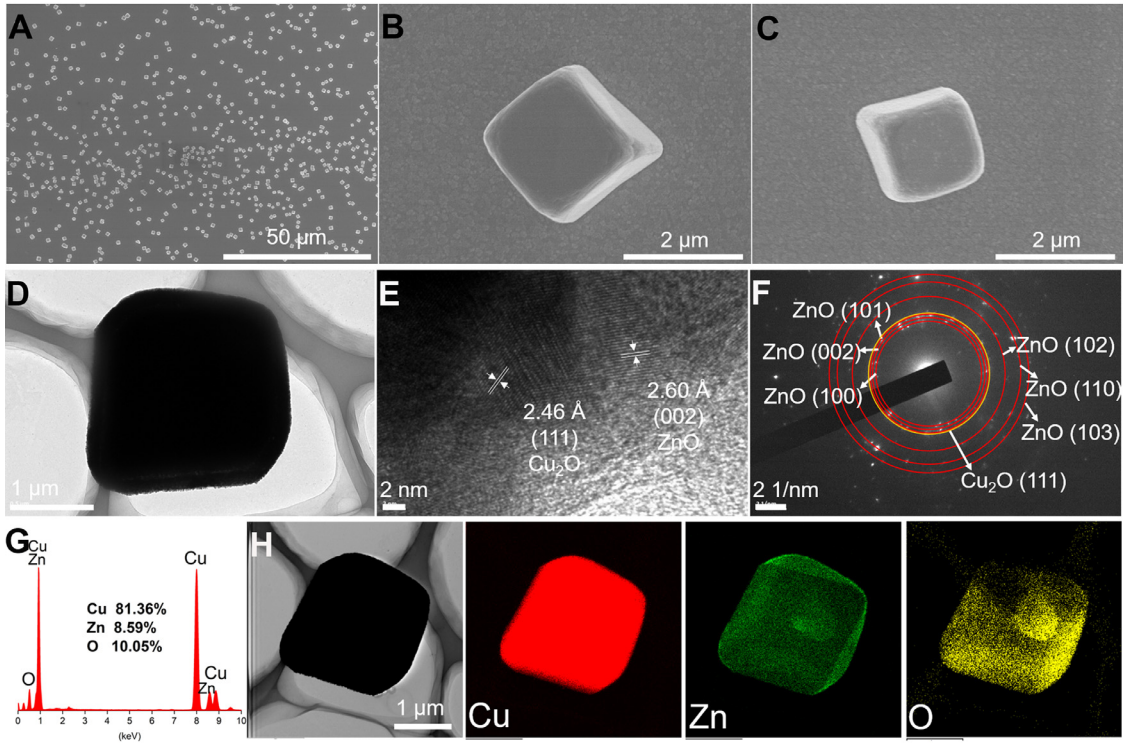

Fig. 2. (A) Low magnification SEM images of ITO-Cu_2O/ZnO (Scale bar, 50 μm); (B, C) High magnification SEM images of ITO-Cu_2O (B), ITO-Cu_2O/ZnO (C) (Scale bar, 2 μm); (D) TEM images of Cu_2O/ZnO (Scale bar, 1 μm); (E) HRTEM images of Cu_2O/ZnO (Scale bar, 2 nm); (F) SAED pattern of Cu_2O/ZnO; (G) EDS detection of Cu_2O/ZnO; (H) Elemental mapping of Cu_2O/ZnO by TEM (Scale bar, 1 μm).

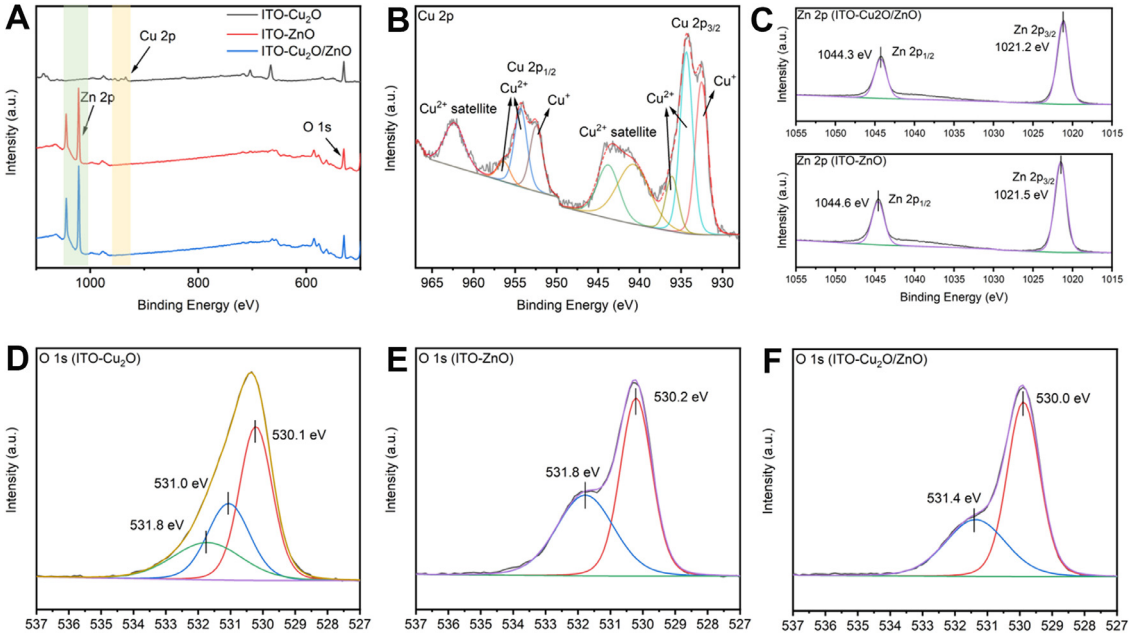

Fig. 3. XPS spectra of as synthesized samples. (A) XPS survey scan; (B) High-resolution of Cu 2p for ITO-Cu_2O; (C) High-resolution of Zn 2p for ITO-ZnO and ITO-Cu_2O/ZnO; (D)–(F) High-solution of O 1s for ITO-Cu_2O (D), ITO-ZnO (E), ITO-Cu_2O/ZnO (F).

nanofilm. In the TEM image, the Cu_2O/ZnO particles also possessed a square morphology with a rough surface (Fig. 2(D)), which corresponded to SEM data. As shown in Fig. 2(E), the high-resolution TEM (HRTEM) images showed lattice fringes of 2.46 and 2.60 Å, corresponding to the d-spacing of the (111) crystal plane of the Cu_2O [39] and the (002) crystal plane of ZnO [40] Fig. 2.(F) showed the SAED pattern of Cu_2O/ZnO. It can be seen from the diffraction ring that ZnO had a polycrystalline structure. The diffraction rings related to ZnO correspond to (100), (002), (101), (102), (110), (103) crystal planes from the inside to the outside. At the same time, the diffraction ring also included the (111) crystal plane of Cu_2O, which corresponded to HRTEM data. As shown in Fig. 2(G), the contents of Cu, Zn, O were 81.36%, 10.05% and 8.59%, respectively. The corresponding mapping data (Fig. 2(H)) showed the uniform distribution of individual elements of Cu, Zn and O. It can be seen from the mapping of Zn element that Zn was evenly wrapped around the particles, which laid the foundation for the formation of Cu_2O and ZnO heterojunctions and the water corrosion protection of materials. This point will be discussed later.

XPS was used to detect the surface information of the sample. As shown in Fig. 3(A), the characteristic peak of Cu 2p was only displayed in the ITO-Cu_2O group, but not in the ITO-Cu_2O/ZnO group, indicating that ZnO was completely covered with Cu_2O. In Fig. 3(B), two bands at 952.5 and 932.5 eV in the Cu 2p spectra can be attributed to Cu(I) 2p1/2 and Cu(I) 2p3/2, respectively [41]. This data proved the existence of Cu_2O. The characteristic peaks at binding energy of 936.2 eV and 934.4 eV corresponded to Cu(II) 2p3/2, and the characteristic peaks at binding energy of 956.4 and 954.3 eV related to Cu(II) 2p1/2 [42,43]. Among them, the two characteristic peaks of 934.4 and 954.3 eV correspond to CuO. Furthermore, two wide satellite peaks attributed to the characteristic shake-up satellite of CuO [44]. CuO might be the result of Cu_2O being oxidized in the air. However, this oxidation process was limited to the surface, which resulted in the relative abundance of CuO being much lower than that of Cu_2O [45]. The two characteristic peaks of 936.2 and 956.4 eV were attributed to the formation of copper hydroxide during the electrodeposition process [46]. As shown in Fig. 3(C), the two strong peaks of Zn 2p can be ascribed to ZnO. The Zn 2p1/2 (1044.3 eV) and 2p3/2 (1021.2 eV) of the ITO-Cu_2O/ZnO group undergone the shift compared to the Zn 2p1/2 (1044.6 eV) and 2p3/2 (1021.5 eV) of ITO-ZnO group, which proved the probable interaction of Cu_2O and CuO with ZnO. The O1s core level spectrum was deconvoluted into two or three peaks. For the O 1s spectra of ITO-Cu_2O, the peaks located at 530.1 eV, 531.0 eV and 531.8 eV can be indexed to the lattice oxygen of Cu_2O, lattice oxygen of ITO and chemisorbed oxygen, respectively (Fig. 3(D)) [47,48]. For the O 1s spectra of ITO-ZnO, the peak located at 530.2 eV and 531.8 eV were assigned to lattice oxygen and chemisorbed oxygen, respectively (Fig. 3(E)) [48]. However, for the O 1s spectrum of the ITO-Cu_2O/ZnO group, the lattice oxygen spectrum of ITO was disappearing, indicating that ZnO covered the entire sample. At the same time, the characteristic binding energy of the lattice oxygen and adsorbed oxygen in ZnO shifted to lower energy, indicating the possible interaction of Cu_2O and CuO with ZnO, which is in accordance with the results of the Zn 2p spectrum (Fig. 3(F)).

The optical absorption capacities of the sample were measured by UV-vis-NIR diffuse reflectance spectroscopy. As shown in Fig. 4(A), the main absorption band of ITO was below 320 nm. The sample of ITO-ZnO has an obvious onset of absorption edge at 390 nm, which indicated that the ZnO nanofilms can only absorb UV light. Compared with the pure ITO group, the absorption of the ITO-Cu_2O and ITO-Cu_2O/ZnO group in the visible light region (400–500 nm) had only a slight improvement. This was because Cu_2O was added to the samples, but Cu_2O did not completely cover the entire ITO. This result was consistent with the light transmittance data. Furthermore, the band gaps of ITO-Cu_2O, ITO-ZnO and ITO-Cu_2O/ZnO are calculated by the transformed Kubelka-Munk formula, which are 2.27 eV, 3.30 eV and 3.22 eV, respectively (Fig. 4(B)). Compared with ITO-ZnO, the band gap of the ITO-Cu_2O/ZnO group was reduced, which was conducive to improving the utilization of sunlight.

A series of photoelectrochemical measurements including transient photocurrent response measurement and EIS were performed to explore the electron transfer process Fig. 5.(A) showed the photocurrent densities of the different samples under solar light irradiation. The photocurrent response of the ITO-Cu_2O/ZnO group was significantly stronger than other groups, indicating a stronger sep-

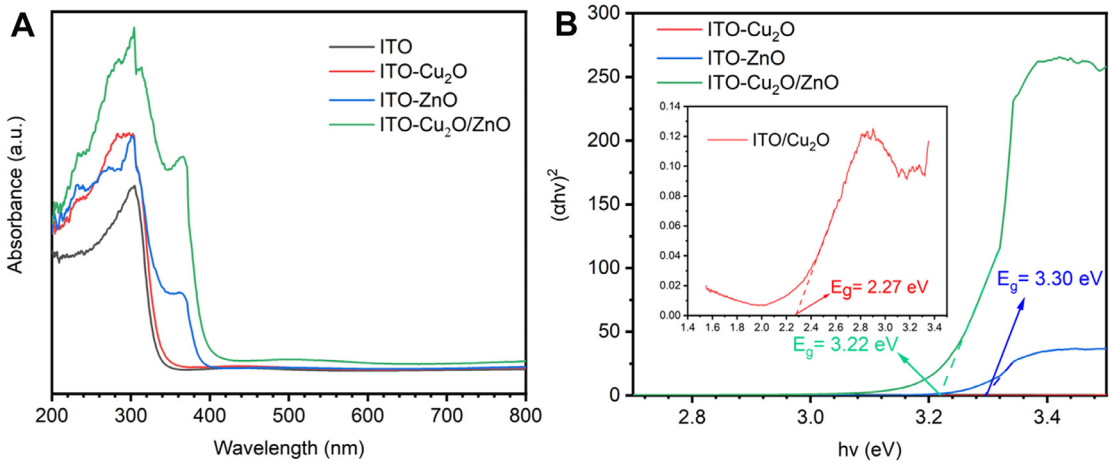

Fig. 4. (A) UV–vis absorption spectra of ITO, ITO-Cu_2O, ITO-ZnO, and ITO-Cu_2O/ZnO; (B) Plots of the $(\alpha h\nu)^2$ versus photon energy ($h\nu$) for ITO-Cu_2O, ITO-ZnO and ITO-Cu_2O/ZnO.

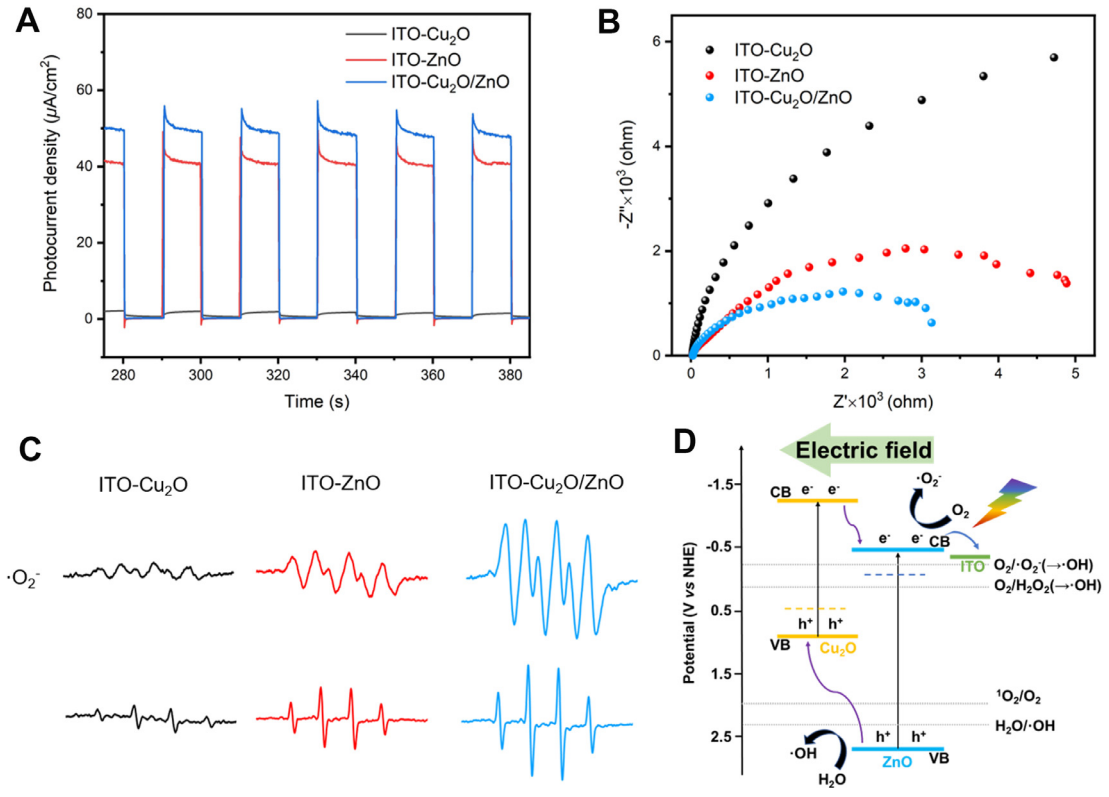

Fig. 5. (A) Transient photocurrent responses, (B) EIS tests, (C) ESR tests of ITO-Cu_2O, ITO-ZnO and ITO-Cu_2O/ZnO; (D) Schematic diagram of the mechanism of enhanced photocatalytic activity.

aration efficiency of electron-hole pairs. EIS measurements were used for studying the interfacial charge transfer resistance between the work electrode and electrolyte. As shown in Fig. 5(B), the ITO-Cu_2O/ZnO group has the smallest semicircle among these three samples, indicating the lowest charge-transfer resistance and highest separation efficiency. Moreover, ESR measurements were performed to examine ROS-generation reactions (Fig. 5(C)). The results showed that ITO-Cu_2O/ZnO samples can produce more ROS including $\bullet O_2^-$ and •OH under the same conditions. This was attributed to the effective separation of photogenerated electron-hole pairs, which corresponded to the photocurrent response and EIS results. ROS can kill bacteria, indicating that this coating material can be applied to surface antibacterial applications.

The proposed mechanism of photocatalysis can be explained as follows. The previous literature reported the conduction band (CB) of Cu_2O (-1.22 eV *vs* NHE) and the valence band (VB) of Cu_2O (0.91 eV *vs* NHE) [48]. Similarly, CB of ZnO (-0.57 eV *vs* NHE) and VB of ZnO (2.59 eV *vs* NHE) had also been reported. As a *p*-type semiconductor, the Fermi level of Cu_2O was closer to VB. Relatively speaking, as a *n*-type semiconductor, the Fermi level of ZnO was closer to CB. As shown in Fig. 5(D), under dark conditions, the Fermi energy level will tend to balance spontaneously when Cu_2O was in contact with ZnO, which leaded to the migration of electrons on ZnO to Cu_2O. A built-in electric field was gradually formed due to the migration of electrons. The formation of the electric field inhibited the continuous migration of electrons, and

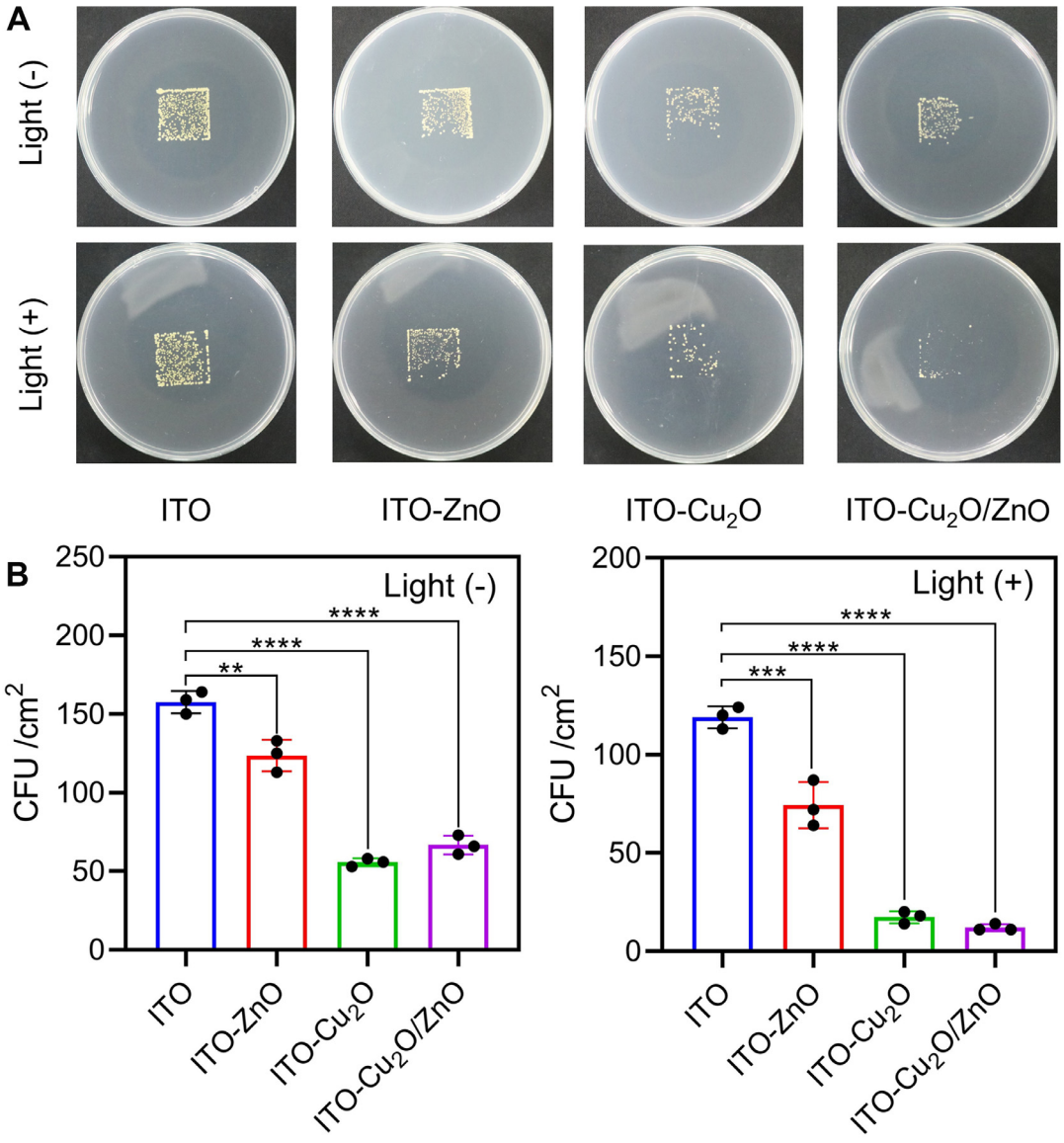

Fig. 6. (A) Spread plates and (B) corresponding strain counts of ITO, ITO-Cu_2O, ITO-ZnO, ITO-Cu_2O/ZnO in the absence and presence of solar light. The error bar means ± standard deviations ($n = 3$ independent samples): $^{**}p < 0.01$, $^{***}p < 0.001$, $^{****}p < 0.0001$.

finally formed a *p-n* heterojunction. Under light irradiation, both substances can produce photogenerated electrons and holes. At the interface, the electrons on the CB of Cu_2O were transferred to the CB of ZnO due to the built-in electric field, whereas the photogenerated holes migrated in the opposite direction [49]. Due to the conductive effect of ITO, the electrons on the CB of ZnO can be transferred to ITO, further promoting the separation of electrons and holes. As a result, the electron transfer process reduced the recombination efficiency of electron-holes pairs. Because the CB edge was more negative than the O_2 reduction reaction potential (-0.33 V for $O_2/•O_2^-$, 0.28 V for O_2/ hydrogen peroxide (H_2O_2)), the electrons accumulated on the CB of ZnO can reduce O_2 to $•O_2^-$ and H_2O_2. The H_2O_2 can further transformed into •OH. Simultaneously, the potentials for water oxidation were lower than the VB of ZnO. Therefore, the holes on ZnO surface can oxide H_2O to •OH. Eventually, the photocatalytic performance was improved due to the electron transfer between the interfaces.

Due to the enhanced photocatalytic performance, we explored the bactericidal ability of the prepared material against *S. aureus*. In Fig. 6(A, B), under dark conditions, ITO-ZnO, ITO-Cu_2O and ITO-Cu_2O/ZnO possessed a certain antibacterial effect (21.6%, 64.7% and 57.8%, respectively) due to the release of zinc ions and copper ions. It is worth noting that the dark sterilization rate of ITO-Cu_2O group was higher than that of ITO-Cu_2O/ZnO group. This was because ZnO nanofilms covered ITO-Cu_2O, which limited the release of copper ions. The ITO-Cu_2O/ZnO samples also had a certain antibacterial effect (> 50%) under dark conditions, indicating the full-time bactericidal ability of the composite material. However, under solar light irradiation, the antibacterial efficiency of ITO-ZnO, ITO-Cu_2O and ITO-Cu_2O/ZnO samples reached 52.7%, 89.2% and 92.5%, respectively. Under light irradiation, the material was excited to produce ROS, which damaged the cell membrane of bacteria and increased the permeability of cell membranes. The damage of the cell membrane will help copper ions and zinc ions quickly enter the inside of bacteria, leading to bacterial metabolic disorders [50]. Based on the ESR data, ITO-Cu_2O/ZnO group had a high ROS yield compare with ITO-Cu_2O sample. Therefore, the ITO-Cu_2O/ZnO samples showed a stronger bactericidal effect than ITO-Cu_2O samples due to the combined action of ROS and copper ions, zinc ions.

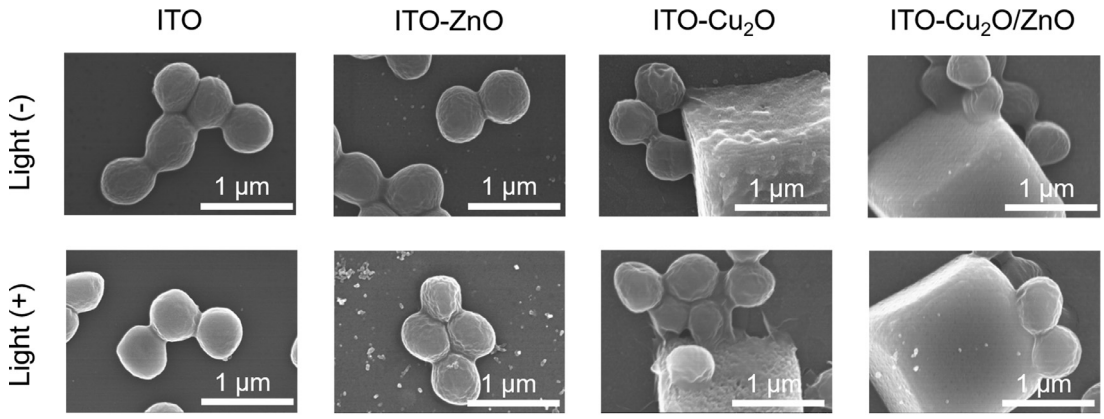

Fig. 7. SEM images for *S. aureus* incubated with different samples of ITO, ITO-Cu_2O, ITO-ZnO and ITO-Cu_2O/ZnO treated with or without light irradiation (Scale bar, 1 μm).

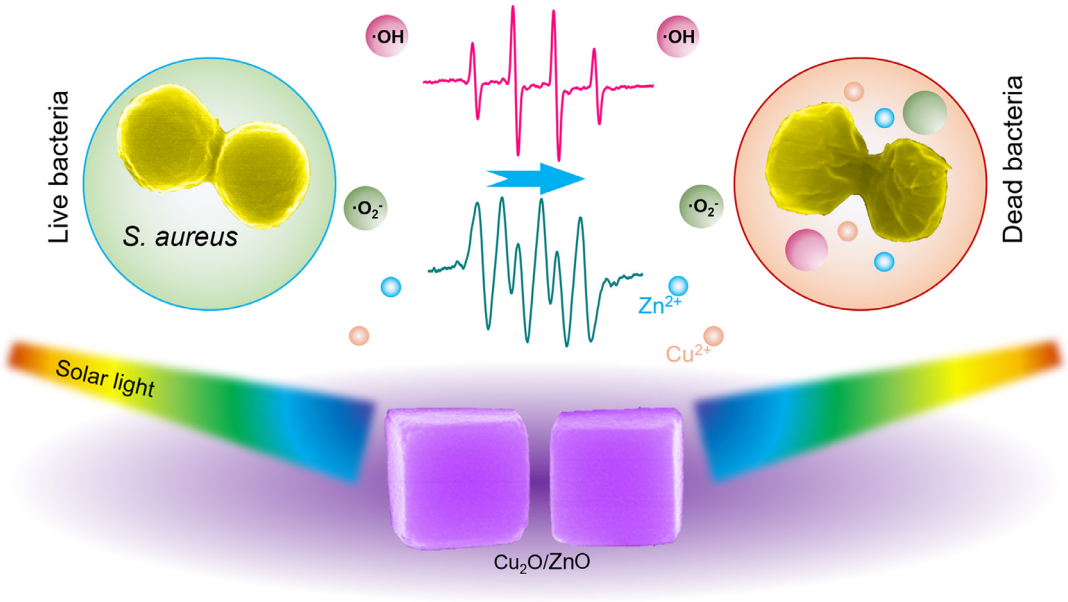

Fig. 8. Scheme of the antibacterial mechanism of photodynamic ion sterilization by the synergistic effect of ROS, released Cu ions and Zn ions.

In order to further understand how the material exerted the antibacterial effect, we had taken the SEM images of *S. aureus* after the antibacterial experiment. As shown in Fig. 7, the bacteria on ITO samples maintained the complete shape with or without light irradiation. But ITO-ZnO, ITO-Cu_2O and ITO-Cu_2O/ZnO samples will shrink slightly without light irradiation. Under solar light irradiation, the ITO-ZnO, ITO-Cu_2O and ITO-Cu_2O/ZnO samples showed different degrees of wrinkles and ruptures, indicating that the bacterial membrane has changed during the sterilization process.

The proposed antibacterial mechanism can be described as follows (Fig. 8). In the dark conditions, Cu_2O and ZnO slowly released copper ions and zinc ions. The interaction of copper ions with the cell membrane leaded to membrane disruption [51]. Furthermore, copper ions caused the inactivation of enzymes. Zinc ions could penetrate cell membranes and accumulate in the body [52]. When the concentration of zinc ions reached a certain level, it could disrupt sugar metabolism and inhibit enzyme activity, and eventually resulted in the death of bacteria. After Cu_2O/ZnO was excited by solar light, the composite materials generated more ROS (•OH and $\bullet O_2^-$). When ROS came into contact with bacteria, the cell wall of the bacteria was destroyed first. At this time, the bacteria can still survive [53]. Later, ROS caused oxidative damage to the bacterial cell membrane. This damage increased the permeability of the cell membrane and leaded to the outflow of bacterial contents [54]. Finally, ROS entered the inside of the bacteria, which caused damage to the protein, and then hindered the bacteria's respiration and other physiological activities [55]. Due to the increased cell membrane permeability, zinc ions and copper ions are more likely to enter the bacteria to exert antibacterial effects. Copper ions and zinc ions can affect the metabolic process of bacteria and cause enzyme inactivation, eventually leading to the death of bacteria [51,52].

Meanwhile, a strange phenomenon was found in the above images. During the sterilization process, the topography of ITO-Cu_2O/ZnO surface became no longer smooth or even rough. In contrast, but the ITO-Cu_2O/ZnO group still kept the original morphology.

In order to understand the nature of this phenomenon, we used PBS solution to simulate the presence of sweat in the actual use environment of antibacterial surface. The groups of ITO-Cu_2O and ITO-Cu_2O/ZnO were soaked in PBS solution for 0 h, 12 h, and 24 h. And then the surface morphology of the samples was observed by SEM. As shown in Fig. 9, the Cu_2O samples (100) crystal planes were divided into small spherical particles, and some small particles had fallen off the surface, forming a part of defects *in situ*. When the time was extended to 24 h, Cu_2O collapsed fur-

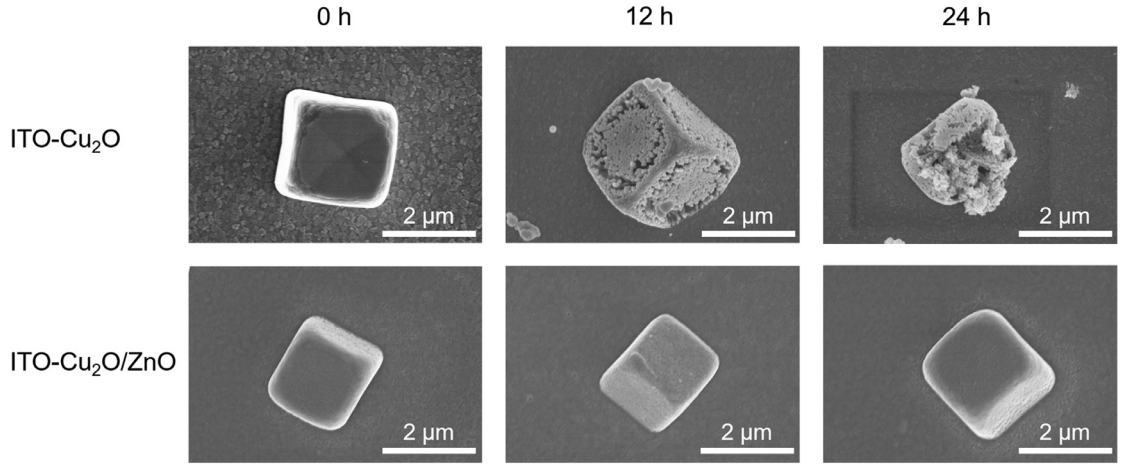

Fig. 9. SEM images of ITO-Cu_2O and ITO-Cu_2O/ZnO after being immersed in PBS solution for 0 h, 12 h and 24 h (Scale bar, 2 μm).

ther and lost the original cube morphology. But when Cu_2O was coated with ZnO nanofilm, the morphology of the material remained unchanged after 24 h of immersion. It showed that ZnO nanofilm prepared by ALD had a certain protective effect on the water corrosion of Cu_2O [56,57]. The prepared Cu_2O exposed (100) crystal plane. It had been reported in the literature that the surface of the (100) crystal plane was a copper atom terminal or an oxygen atom terminal [58]. In either case, the copper and oxygen atoms on the surface were coordination unsaturated, which can easily coordinate with the ions in the PBS aqueous solution, weakening the Cu-O bond, and then causing corrosion. However, after ZnO nanofilm was deposited by ALD, the surface of the material was covered with a conformal ZnO nanofilm [59]. Since the water molecule finished the ALD cycles at the end, the outermost layer was the H atom terminal. The outer layer atoms are all coordination saturated, so the corrosion phenomenon was greatly slowed down.

4. Conclusions

In summary, an ITO-Cu_2O/ZnO based photodynamic ions antibacterial system with high light transmittance was successfully prepared by electrodeposition and ALD method, in which Cu_2O and ZnO formed a *p-n* heterojunction. Compared with ITO-Cu_2O and ITO-ZnO, the photocatalytic performance of ITO-Cu_2O/ZnO was significantly improved. This was attributed to the rapid migration of electrons between the interfaces, which promoted the separation of photogenerated electrons and holes. Due to the synergy of ROS, copper ions and zinc ions, the ITO-Cu_2O/ZnO samples achieved 92.5% sterilization effect. At the same time, the material still had a certain sterilization effect under dark conditions, ensuring the full-time sterilization of the hand touching surface. In addition, the coating of ZnO had a protective effect on the water corrosion of Cu_2O and prolonged the service life of the hybrid film. We expect that this work will provide a new solution for imparting antibacterial properties to the hand touching surface.

Declaration of Competing Interest

The authors declare that they have no known competing financial interests or personal relationships that could have appeared to influence the work reported in this paper.

Acknowledgments

This work was jointly supported by the National Natural Science Foundation of China (Nos. 51871162, and 52173251), and the China National Funds for Distinguished Young Scientists (No.51925104).

Supplementary materials

Supplementary material associated with this article can be found, in the online version, at doi:10.1016/j.jmst.2021.12.064.

References

[1] T.A.P. da Fonseca, R. Pessôa, A.C. Felix, S.S. Sanabani, Int. J. Environ. Res. Public Health 13 (2016) 152.
[2] D. Vargas-Robles, C. Gonzalez-Cedillo, A.M. Hernandez, L.D. Alcaraz, M. Peimbert, Plos One 15 (2020) e0237272.
[3] P. Rahi, R. Kurli, A.N. Pansare, M. Khairnar, S. Jagtap, N.B. Patel, S.G. Dastager, P.A. Lawson, Y.S. Shouche, Int. J. Syst. Evol. Microbiol. 68 (2018) 1052–1058.
[4] K. Hayashi, I. Mori, K. Takeda, Y. Okada, A. Hayase, T. Mori, Y. Nishioka, K. Manabe, Skin Res. Technol. (2021), doi:10.1111/srt.13078.
[5] D. Xu, T.Y. Wang, Z.Y. Lu, Y.Q. Wang, B. Sun, S.D. Wang, Q. Fu, Z.G. Bi, S. Geng, J. Mater. Sci. Technol. 90 (2021) 133–142.
[6] N. Fierer, M. Hamady, C.L. Lauber, R. Knight, Proc. Natl. Acad. Sci. USA. 105 (2008) 17994–17999.
[7] P.N. Zivich MPH, A.S. Gancz, A.E. Aiello, Am. J. Infect. Control 46 (2018) 448–455.
[8] H. Choi, P. Chatterjee, E. Lichtfouse, J.A. Martel, M. Hwang, C. Jinadatha, V.K. Sharma, Environ. Chem. Lett. 19 (2021) 1945–1951.
[9] J.M. Boyce, Antimicrob. Resist. Infect. Control 5 (2016) 10.
[10] D.L. Han, Y. Li, X.M. Liu, K.W.K. Yeung, Y.F. Zheng, Z.D. Cui, Y.Q. Liang, Z.Y. Li, S.L. Zhu, X.B. Wang, S.L. Wu, J. Mater. Sci. Technol. 62 (2021) 83–95.
[11] Q.Y. Zheng, X.M. Liu, Y.F. Zheng, K.W.K. Yeung, Z.D. Cui, Y.Q. Liang, Z.Y. Li, S.L. Zhu, X.B. Wang, S.L. Wu, Chem. Soc. Rev. 50 (2021) 5086–5125.
[12] J. Song, J. Li, X.R. Bai, L. Kang, L.Y. Ma, N.Q. Zhao, S.L. Wu, Y. Xue, J.J. Li, X.J. Ji, J.W. Sha, J. Mater. Sci. Technol. 87 (2021) 83–94.
[13] Y. Zou, Y.X. Zhang, Q. Yu, H. Chen, J. Mater. Sci. Technol. 70 (2021) 24–38.
[14] X.Y. Kong, X.M. Liu, Y.F. Zheng, P.K. Chu, Y. Zhang, S.L. Wu, Mater. Sci. Eng. R Rep. 145 (2021) 100610.
[15] R. Lv, Y.Q. Liang, Z.Y. Li, S.L. Zhu, Z.D. Cui, S.L. Wu, Rare Met. (2021), doi:10.1007/s12598-021-01759-4.
[16] Q. Wu, X.M. Liu, B. Li, L. Tan, Y. Han, Z.Y. Li, Y.Q. Liang, Z.D. Cui, S.L. Zhu, S.L. Wu, Y.F. Zheng, J. Mater. Sci. Technol. 67 (2021) 70–79.
[17] B.Y. Li, I.S. Kim, S.H. Dai, M.N. Sarwar, X.H. Yang, Colloid Interface Sci. Commun. 45 (2021) 100543.
[18] S.T. Wang, Y. Fang, Z.Q. Zhang, Q. Jin, J. Ji, Colloid Interface Sci. Commun. 40 (2021) 100354.
[19] T. Wei, Q. Yu, H. Chen, Adv. Healthc. Mater. 8 (2019) 1801381.
[20] Y.M. Xiang, J. Li, X.M. Liu, Z.D. Cui, X.J. Yang, K.W.K. Yeung, H.B. Pan, S.L. Wu, Mater. Sci. Eng. C Mater. Biol. Appl. 79 (2017) 629–637.
[21] K. Su, L. Tan, X.M. Liu, Z.D. Cui, Y.F. Zheng, B. Li, Y. Han, Z.Y. Li, S.L. Zhu, Y.Q. Liang, X.B. Feng, X.B. Wang, S.L. Wu, ACS Nano 14 (2020) 2077–2089.
[22] W. Guan, L. Tan, X.M. Liu, Z.D. Cui, Y.F. Zheng, K.W.K. Yeung, D. Zheng, Y.Q. Liang, Z.Y. Li, S.L. Zhu, X.B. Wang, S.L. Wu, Adv. Mater. 33 (2021) 2006047.
[23] Y. Yu, L. Tan, Z.Y. Li, X.M. Liu, Y.F. Zheng, X.B. Feng, Y.Q. Liang, Z.D. Cui, S.L. Zhu, S.L. Wu, ACS Nano 15 (2021) 10628–10639.

[24] H.P. Liu, J.F. Li, X.M. Liu, Z.Y. Li, Y. Zhang, Y.Q. Liang, Y.F. Zheng, S.L. Zhu, Z.D. Cui, S.L. Wu, ACS Nano 15 (2021) 18505–18519.
[25] Y.Q. Qiao, X.M. Liu, B. Li, Y. Han, Y.F. Zheng, K.W.K. Yeung, C.Y. Li, Z.D. Cui, Y.Q. Liang, Z.Y. Li, S.L. Zhu, X.B. Wang, S.L. Wu, Nat. Commun. 11 (2020) 4446.
[26] J.N. Fu, Y. Li, Y. Zhang, Y.Q. Liang, Y.F. Zheng, Z.Y. Li, S.L. Zhu, C.Y. Li, Z.D. Cui, S.L. Wu, Adv. Mater. 33 (2021) e2102926.
[27] S.B. Wei, Y.Q. Qiao, Z.C. Wu, X.M. Liu, Y. Li, Z.D. Cui, C.Y. Li, Y.F. Zheng, Y.Q. Liang, Z.Y. Li, S.L. Zhu, H.R. Wang, X.B. Wang, R.C. Che, S.L. Wu, Nano Today 37 (2021) 101090.
[28] J. Li, X.M. Liu, L. Tan, Z.D. Cui, X.J. Yang, Y.Q. Liang, Z.Y. Li, S.L. Zhu, Y.F. Zheng, K.W.K. Yeung, X.B. Wang, S.L. Wu, Nat. Commun. 10 (2019) 4490.
[29] Y.D. Xu, X.M. Liu, Y.F. Zheng, C.Y. Li, K.W.K. Yeung, Z.D. Cui, Y.Q. Liang, Z.Y. Li, S.L. Zhu, S.L. Wu, Bioact. Mater. 6 (2021) 1575–1587.
[30] G. Hazell, P.W. May, P. Taylor, A.H. Nobbs, C.C. Welch, B. Su, Biomater. Sci. 6 (2018) 1424–1432.
[31] J.P. Celli, B.Q. Spring, I. Rizvi, C.L. Evans, K.S. Samkoe, S. Verma, B.W. Pogue, T. Hasan, Chem. Rev. 110 (2010) 2795–2838.
[32] Y. Yang, X.Z. Wu, L. Ma, C. He, S.J. Cao, Y.P. Long, J.B. Huang, R.D. Rodriguez, C. Cheng, C.S. Zhao, L. Qiu, Adv. Mater. 33 (2021) 202005477.
[33] F. Cieplik, D.M. Deng, W. Crielaard, W. Buchalla, E. Hellwig, A. Al-Ahmad, T. Maisch, Crit. Rev. Microbiol. 44 (2018) 571–589.
[34] X.T. Shi, C.W. Xue, F. Fang, X.W. Song, F. Yu, M.X. Liu, Z.P. Wei, X. Fang, D.X. Zhao, H.B. Xin, X.L. Wang, ACS Appl. Mater. Interfaces 8 (2016) 8386–8392.
[35] J.F. Ma, K. Wang, L.Y. Li, T. Zhang, Y. Kong, S. Komarneni, Ceram. Int. 41 (2015) 2050–2056.
[36] H.J. Li, Y. Zhou, W.G. Tu, J.H. Ye, Z.G. Zou, Adv. Funct. Mater. 25 (2015) 998–1013.
[37] J.S. Luo, S.D. Tilley, L. Steier, M. Schreier, M.T. Mayer, H.J. Fan, M. Gratzel, Nano Lett. 15 (2015) 1395–1402.
[38] Y.G. Gao, Q. Wu, X.Z. Liang, Z.Y. Wang, Z.K. Zheng, P. Wang, Y.Y. Liu, Y. Dai, M.H. Whangbo, B.B. Huang, Adv. Sci. 7 (2020) 1902820.
[39] X.J. Yu, J. Zhang, J. Zhang, J.F. Niu, J. Zhao, Y.C. Wei, B.H. Yao, Chem. Eng. J. 374 (2019) 316–327.
[40] J. Li, X.M. Liu, L. Tan, Y.Q. Liang, Z.D. Cui, X.J. Yang, S.L. Zhu, Z.Y. Li, Y.F. Zheng, K.W.k. Yeung, X.B. Wang, S.L. Wu, Small Methods 3 (2019) 1900048.
[41] M.M. Zhang, J.J. Wang, Y. Wang, J.F. Zhang, X.P. Han, Y.N. Chen, Y.S. Wang, Z. Karim, W.B. Hu, Y.D. Deng, J. Mater. Sci. Technol. 62 (2021) 119–127.
[42] A. Celik-Kucuk, T. Abe, J. Power Sources 496 (2021) 229828.
[43] S.S. Xin, G.C. Liu, X.H. Ma, J.X. Gong, B.R. Ma, Q.H. Yan, Q.H. Chen, D. Ma, G.S. Zhang, M.C. Gao, Y.J. Xin, Appl. Catal. B Environ. 280 (2021) 119386.
[44] Y.C. Chen, Y.J. Chen, P.H. Dong, Y.K. Hsu, ACS Appl. Energ. Mater. 3 (2020) 1373–1380.
[45] Y.C. Chen, P.H. Dong, Y.K. Hsu, ACS Appl. Mater. Interfaces 13 (2021) 38375–38383.
[46] J.Y. Lin, C.C. Wan, Y.Y. Wang, J.C. Chen, J.Y. Lai, Y.D. Fan, J.P. Chuang, J. Electrochem. Soc. 154 (2007) H530–H535.
[47] F.C. Lei, Y.F. Sun, K.T. Liu, S. Gao, L. Liang, B.C. Pan, Y. Xie, J. Am. Chem. Soc. 136 (2014) 6826–6829.
[48] F. Zhang, Y.H. Li, M.Y. Qi, Z.R. Tang, Y.J. Xu, Appl. Catal. B Environ. 268 (2020) 118380.
[49] P.F. Xia, S.W. Cao, B.C. Zhu, M.J. Liu, M.S. Shi, J.G. Yu, Y.F. Zhang, Angew. Chem. Int. Ed. 59 (2020) 5218–5225.
[50] J. Li, S. Song, J.S. Meng, L. Tan, X.M. Liu, Y.F. Zheng, Z.Y. Li, K.W.K. Yeung, Z.D. Cui, Y.Q. Liang, S.L. Zhu, X.C. Zhang, S.L. Wu, J. Am. Chem. Soc. 143 (2021) 15427–15439.
[51] C. Molteni, H.K. Abicht, M. Solioz, Appl. Environ. Microbiol. 76 (2010) 4099–4101.
[52] J. Li, L. Tan, X.M. Liu, Z.D. Cui, X.J. Yang, K.W.K. Yeung, P.K. Chu, S.L. Wu, ACS Nano 11 (2017) 11250–11263.
[53] H. Zheng, P.C. Maness, D.M. Blake, E.J. Wolfrum, S.L. Smolinski, W.A. Jacoby, J. Photochem. Photobiol. A Chem. 130 (2000) 163–170.
[54] X.Y. Zhang, G.N. Zhang, H.Y. Zhang, X.P. Liu, J. Shi, H.X. Shi, X.H. Yao, P.K. Chu, X.Y. Zhang, Chem. Eng. J. 382 (2020) 122849.
[55] Y. Li, X.M. Liu, L. Tan, Z.D. Cui, D.D. Jing, X.J. Yang, Y.Q. Liang, Z.Y. Li, S.L. Zhu, Y.F. Zheng, K.W.K. Yeung, D. Zheng, X.B. Wang, S.L. Wu, Adv. Funct. Mater. 29 (2019) 1900946.
[56] A. Paracchino, V. Laporte, K. Sivula, M. Gratzel, E. Thimsen, Nat. Mater. 10 (2011) 456–461.
[57] A. Paracchino, N. Mathews, T. Hisatomi, M. Stefik, S.D. Tilley, M. Gratzel, Energy Environ. Sci. 5 (2012) 8673–8681.
[58] C. Gattinoni, A. Michaelides, Surf. Sci. Rep. 70 (2015) 424–447.
[59] T. Tynell, M. Karppinen, Semicond. Sci. Technol. 29 (2014) 043001.